Title

Electron confinement by laser-driven azimuthal magnetic fields during direct laser acceleration

Journal

Physics of Plasmas, 27(5)

ISSN

1070-664X

Authors

Wang, Tao
Gong, Zheng
Arefiev, Alexey

Publication Date

2020-05-01

DOI

10.1063/5.0006295

Peer reviewed

Electron confinement by laser-driven azimuthal magnetic fields during direct laser acceleration

T. Wang,[1,2] Z. Gong,[3,4] and A. Arefiev[1,2]
[1)] *Department of Mechanical and Aerospace Engineering, University of California at San Diego, La Jolla, CA 92093*
[2)] *Center for Energy Research, University of California at San Diego, La Jolla, CA 92093*
[3)] *Center for High Energy Density Science, The University of Texas, Austin, TX 78712*
[4)] *SKLNPT, KLHEDP, and CAPT, School of Physics, Peking University, Beijing 100871, China*

(Dated: 3 March 2020)

A laser-driven azimuthal plasma magnetic field is known to facilitate electron energy gain from the irradiating laser pulse. The enhancement is due to changes in the orientation between the laser electric field and electron velocity caused by magnetic field deflections. Transverse electron confinement is critical for realizing this concept experimentally. We find that the phase velocity of the laser pulse has a profound impact on the transverse size of electron trajectories. The transverse size remains constant below a threshold energy that depends on the degree of the superluminosity and it increases with the electron energy above the threshold. This increase can cause electron losses in tightly focused laser pulses. We show using 3D particle-in-cell simulations that the electron energy gain can be significantly increased by increasing laser power at fixed intensity due to the increased electron confinement. This finding makes a strong case for designing experiments at multi-PW laser facilities.

Direct laser acceleration is one of fundamental mechanisms for transferring energy from an intense laser pulse to electrons of a laser-irradiated plasma. At relativistic laser intensities, most of the transferred energy is associated with the forward rather than transverse motion. This aspect has been successfully exploited for the development of secondary particle (ion[1,2], neutron[3,4], positron[5–7]) and radiation sources[8–10] that have multiple inter-disciplinary applications.

There are two important aspects that distinguish direct laser acceleration in a plasma from that in a vacuum. In a vacuum, a laser beam of a finite width expels electrons radailly during the acceleration process. This limits the acceleration time for a given electron. Increased transverse velocity also increases electron dephasing from the laser pulse, which negatively impacts the energy gain. As the laser propagates through a plasma, it generates quasi-static radial electric and azimuthal magnetic fields[11]. These fields can provide electron confinement within the laser beam, leading to a significant increase in electron energy[12]. It is worth mentioning that the energy gain is further facilitated by transverse electron deflections that alter electron dephasing[13].

The energy enhancement in the presence of the quasi-static plasma electric and magnetic fields is a threshold process[14]. It has been previously established that the threshold depends on laser amplitude[11], plasma field strength, and electron momentum at the start of the acceleration process (e.g. see Refs. 11, 13–15). In experimentally relevant configurations, the width of the laser pulse is another important parameter that must be taken into consideration.

In this work, we examine the conditions for the transverse electron confinement and show that the confinement strongly depends on $v_{ph} - c$, where v_{ph} is the phase velocity and c is the speed of light. This parameter characterizes the degree of superluminosity. We find that the amplitude of transverse electron displacements is limited during the energy gain process only while the energy remains below a specific threshold value. Once the energy exceeds the threshold value, the transverse displacements begin to grow with energy. This increase in displacement can lead to particle losses and premature termination of the energy gain process in a tightly focused laser pulse.

In order to explore the impact of the laser pulse width on laser-driven electron acceleration, we have performed two 3D particle-in-cell (PIC) simulations for 1 and 4 PW laser pulses irradiating a uniform plastic target. The laser power is increased by increasing the laser energy and the size of the focal spot w_0 while keeping the peak intensity of $5{\times}10^{22}$ W/cm^2 and the pulse duration of 35 fs fixed. The parameters of the laser pulse, the target density, and other simulation parameters are shown in Table I. The electron density in the target is much higher than the classical critical density defined as $n_{cr} \equiv m_e\omega^2/(4\pi e^2)$, where m_e and e are the electron mass and charge, and ω is the frequency of the laser pulse. We find that the laser pulse is able to propagate through the target in both cases due to its high intensity that makes the plasma relativistically transparent. The transparency condition, $n_e \ll a_0 n_{cr}$, is defined using a dimensionless parameter that we refer to as the normalized laser amplitude $a_0 \equiv |e|E_0/(m_e c\omega)$, where E_0 is the peak amplitude of the laser electric field and c is the speed of light. It is well satisfied for the considered parameters.

Figure 1 shows snapshots of the electron spectra at $t = 69$ fs for the 1 PW run and at $t = 72$ fs for the 4 PW run. We define $t = 0$ fs as the time when the laser pulse reaches its peak intensity in the focal plane in the absence of the target. It is evident that the laser-accelerated electrons are able to achieve much higher energy at higher laser power. We have verified that changes in laser inten-

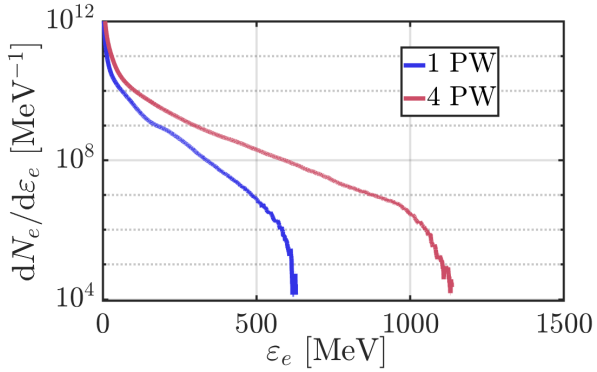

FIG. 1: Snapshots of electron spectra from 3D PIC simulations taken when the electrons reach the highest cutoff energy ε_{max} ($t = 69$ fs for 1 PW and $t = 72$ fs for 4 PW).

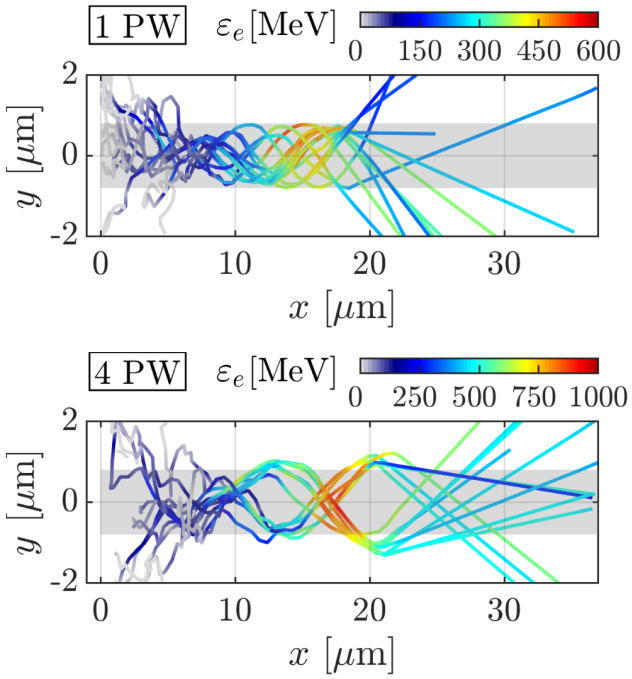

FIG. 2: Representative trajectories of energetic electrons: the upper panel is for 1 PW and the lower panel is for 4 PW. At each power, we randomly selected the same number of electrons with energies within $[2\varepsilon_{max}/3, \varepsilon_{max}]$, where ε_{max} is the maximum cutoff energy from Fig. 1. The shaded area that is 1.6 μm wide is added to provide a an easy reference for the amplitude of transverse electron oscillations.

sity inside the plasma are not sufficient to explain such a dramatic increase.

We have tracked energetic electrons in both runs to identify the changes in electron trajectories associated with the power increase. To make an unbiased selection for each power, we randomly chose the same number of electrons with energies in the range between $(2/3)\varepsilon_{max}$ and ε_{max}. We define ε_{max} as the maximum cutoff electron energy achieved during each run. The spectra that determine ε_{max} at 1 and 4 PW are shown in Fig. 1, with $\varepsilon_{max} = 610$ MeV for 1 PW and $\varepsilon_{max} = 1100$ MeV for

TABLE I: Parameters used in the 3D PIC simulations

3D PIC simulation parameters	
Laser pulse:	
Pulse energy	37 and 149 J
Peak intensity	5×10^{22} W/cm^2
a_0	190
Polarization	linearly along $\hat{\mathbf{y}}$
Wavelength	$\lambda = 1$ μm
Power	$P = 1$ and 4 PW
Location of the focal plane	$x = 0$ μm
Pulse profile (transverse & longitudinal)	Gaussian
Pulse duration (FHWM for intensity)	35 fs
Pulse width/focal spot (FWHM for intensity)	$w_0 = 1.3$ and 2.7 μm
Plasma:	
Composition	carbon ions and electrons
Target thickness	$d = 4.0$ and 5.0 μm
Electron density	$n_e = 20\ n_{cr}$
Ionization state of carbon	fully ionized
Target length	$L = 35$ μm
General parameters:	
Spatial resolution	30/μm ×30/μm ×30/μm
# of macro-particles/cell	
Electrons	15
Carbon ions	5

4 PW. Figure 2 shows the trajectories of the tracked electrons and their energy (shown in color) for the 1 and 4 PW runs. The tracking reveals that energetic electrons are lost from the 1 PW laser pulse at an earlier moment. In the 4 PW run, the electrons remain in the laser pulse longer, which allows them to gain more energy from the laser field. The energy increase is correlated with an increase in the amplitude of transverse displacements. These results suggest that transverse electron confinement plays a significant role in determining the electron energy gain and thus the electron spectrum.

In the presented simulations, we observe a strong slowly evolving azimuthal magnetic field that forms a magnetic filament whose transverse size is comparable to the width of the laser pulse. The magnetic field is sustained by a longitudinal electron current that is caused by the propagating laser pulse. The plasma magnetic field in our simulations is strong because of the high electron density in the target that is able to support a strong longitudinal electron current. The field of the filament deflects forward moving moving electrons towards the axis of the laser pulse providing transverse electron confinement. It is convenient to introduce a concept of the magnetic boundary, which is the boundary where a considered electron stops its transverse motion due to the deflection by the plasma magnetic field. The magnetic boundary must be within the magnetic filament to ensure transverse electron confinement during the energy gain.

Our goal is to find out what sets the location of the magnetic boundary. Motivated by the presented simulations, we consider a reduced model where a test elec-

tron is subjected to prescribed time-dependent fields of the laser and static fields of the channel. Our approach to finding the magnetic boundary is to assume that the laser beam and the magnetic filament are much wider than the magnetic boundary. We therefore approximate the laser by a plane electromagnetic wave with a superluminal phase velocity $v_{ph} > c$. The phase velocity in such a model can be used to account for the presence of the plasma and for the fact that the laser pulse has a finite width. In order to simplify our analytical derivations, we assume that the magnetic filament is sustained by a longitudinal current with a uniform current density j_0.

The electron dynamics is described by the following equations:

$$\frac{d\boldsymbol{p}}{dt} = -|e|\boldsymbol{E} - \frac{|e|}{\gamma m_e c}\left[\boldsymbol{p}\times\boldsymbol{B}\right], \tag{1}$$

$$\frac{d\boldsymbol{r}}{dt} = \frac{c}{\gamma}\frac{\boldsymbol{p}}{m_e c}, \tag{2}$$

where the electric and magnetic fields ($\boldsymbol{E}$ and $\boldsymbol{B}$) are given. Here $\gamma = \sqrt{1+p^2/m_e^2c^2}$ is the relativistic γ-factor, $\boldsymbol{r}$ and $\boldsymbol{p}$ are the electron position and momentum, and t is the time. In the regime under consideration, $\boldsymbol{E} = \boldsymbol{E}_{wave}$ is just the laser electric field, whereas $\boldsymbol{B} = \boldsymbol{B}_{wave}+\boldsymbol{B}_{filament}$ is a superposition of the magnetic fields of the wave and the filament. Without any loss of generality, we consider a linearly polarized wave propagating in the positive direction along the x-axis with

$$\boldsymbol{E}_{wave} = \boldsymbol{e}_y E_0\cos(\xi), \tag{3}$$

$$\boldsymbol{B}_{wave} = \boldsymbol{e}_z\frac{c}{v_{ph}}E_0\cos(\xi), \tag{4}$$

where E_0 is the wave amplitude and

$$\xi = \omega_0 t - \omega_0 x/v_{ph} \tag{5}$$

is the phase variable. The magnetic field of the channel sustained by the current density $\boldsymbol{j} = j_0\boldsymbol{e}_x$ is given by

$$\boldsymbol{B}_{filament} = \frac{m_e c^2}{|e|}\nabla\times\boldsymbol{a}_{filament}, \tag{6}$$

where

$$\boldsymbol{a}_{filament} = \boldsymbol{e}_x\alpha\left(y^2+z^2\right)/\lambda_0^2, \tag{7}$$

$$\alpha \equiv -\pi\lambda_0^2|e|j_0/m_e c^3, \tag{8}$$

and $\lambda_0 \equiv 2\pi c/\omega_0$ is the vacuum wavelength. The filament that confines electrons has $j_0 < 0$.

It can be verified using the equations of motion that the following quantity remains conserved as the electron moves in the considered field configuration:

$$\gamma - \frac{v_{ph}}{c}\frac{p_x}{m_e c} + \frac{v_{ph}}{c}a_{filament} = C. \tag{9}$$

We are going to consider a relativistic electron that is starting its motion on axis while moving in transverse direction. We specifically set

$$p_y = p_i, \tag{10}$$

$$p_z = 0 \tag{11}$$

at $\xi = 0$ to mimic the electron injection into the magnetic filament observed in kinetic simulations[10]. The constant of motion for this electron is its initial γ-factor γ_i:

$$C = \gamma_i \equiv \sqrt{1+p_i^2/m_e^2c^2}. \tag{12}$$

We first examine the electron dynamics in the absence of the laser field. In this case, the total momentum of the electron is conserved, which means that $C = \gamma$. We then find from Eq. (9) that

$$\frac{p_x}{m_e c} = a_{filament}. \tag{13}$$

There are two features of the electron dynamics that are evident from this relation. If $j_0 < 0$ and $a_{filament} \geq 0$, then the electron slides forward along the filament instead of performing rotations around a fixed axial location, since $p_x \geq 0$. The transverse displacements are constrained by the magnetic field,

$$y \leq \lambda_0\left(\frac{p_i}{\alpha m_e c}\right)^{1/2}, \tag{14}$$

with the corresponding limit obtained from Eq. (13) by setting $p_x = p_i$.

In the presence of the laser, the electron can gain energy from the laser field. In order to find how this impacts the radial confinement, we re-write Eq. (9) as

$$ua_{filament} = \gamma_i - \left[\gamma - \frac{p_x}{m_e c}\right] + (u-1)\frac{p_x}{m_e c}. \tag{15}$$

where we introduced

$$u \equiv v_{ph}/c \tag{16}$$

for compactness. As the longitudinal momentum and the γ-factor increase, the condition $\gamma - p_x/m_e c > 0$ must hold. Moreover, we have $u - 1 \geq 0$. The maximum transverse displacement is achieved in the limit of $\gamma - p_x/m_e c \to 0$. In this limit, we can replace $p_x/m_e c$ with γ in the last term, which yields

$$|y| \leq r_{\rm MB} \equiv \frac{\lambda_0}{\sqrt{\alpha u}}\left[\gamma_i + (u-1)\gamma\right]^{1/2}. \tag{17}$$

The right-hand side defines the radial location, $r = r_{\rm MB}$, of the magnetic boundary. The trajectory remains confined within the magnetic boundary as the electron gains energy from the laser pulse.

We characterize electron energy gain by the ratio γ/γ_i and define two limiting cases based on the value of this parameter. If

$$\gamma/\gamma_i \ll (u-1)^{-1}, \tag{18}$$

then we have

$$r_{\rm MB} \approx \lambda_0\sqrt{\gamma_i/\alpha u} \tag{19}$$

In the opposite regime of $\gamma/\gamma_i \gg (u-1)^{-1}$, we have

$$r_{\rm MB} \approx \lambda_0\sqrt{\frac{u-1}{\alpha u}}\gamma^{1/2}. \tag{20}$$

We then conclude that the location of the magnetic boundary remains constant and given by Eq. (19) until the electron energy exceeds $\gamma \approx \gamma_i/(u-1)$. Above this threshold, the magnetic boundary expands, $r_{MB} \propto \gamma^{1/2}$, as the electron energy increases.

We have so far assumed that the magnetic field of the filament is much stronger than the radial quasistatic plasma electric field that arises due to charge separation. Such a regime has been observed in PIC simulations at $a_0 \gg 1$ and $n_e \gg n_{cr}$ [16]. At lower a_0 and lower plasma densities, the electric field can become comparable to or even stronger than the magnetic field[11]. Our results can be easily generalized to such a regime. We assume that the radial electric field is generated by a uniform charge density distribution ρ. It can be verified using the equations of motion that include this field that the following quantity remains conserved:

$$\gamma - \frac{v_{ph}}{c}\frac{p_x}{m_e c} + \frac{v_{ph}}{c}a_{filament} + \frac{\omega_{p0}^2 r^2}{4c^2}\frac{\rho}{|e|n_0} = C, \quad (21)$$

where n_0 is the original electron density in the plasma, $\omega_{p0}^2 = 4\pi n_0 e^2/m_e$ is the corresponding electron plasma frequency, and $r = \sqrt{y^2+z^2}$ is the radius in a cylindrical system of coordinates whose axis is aligned with that of the channel. We now take into account Eq. (7) to obtain that

$$\gamma - \frac{v_{ph}}{c}\frac{p_x}{m_e c} + \kappa\alpha u\frac{r^2}{\lambda_0^2} = C, \quad (22)$$

where

$$\kappa \equiv 1 - \rho c^2/v_{ph} j_0. \quad (23)$$

In the limit of $\rho \to 0$, $\kappa = 1$ and Eq. (22) reduces to Eq (9).

In order to generalize the results given by Eqs. (17), (19), and (20), all we need to do is replace α by $\kappa\alpha$, where κ must be calculated based on the current and charge density in the filament. We can conclude that the magnetic field plays a major role in determining the electron dynamics if $\kappa \approx 1$, which is equivalent to the following condition

$$|\rho|c^2 \ll v_{ph}|j_0|. \quad (24)$$

If $\rho > 0$ and $j_0 < 0$, then both the electric and magnetic fields confine the electron. This causes the radius of the magnetic boundary to become smaller, but it is important to stress that the energy enhancement threshold remains unchanged.

We conclude our discussion by applying the above theory to examine the electron motion in our 3D kinetic simulations. For both 1 PW and 4 PW simulations, the current densities are similar and approximately 8×10^{17} A/m^2, corresponding to $\alpha \approx 147$. The phase velocity can be calculated from Fig. 3 where the laser field on the central axis ($y = z = 0$) is plotted in a moving window as a function of time. For 1 PW, $v_{ph} \approx 1.082c$ and for 4 PW, $v_{ph} \approx 1.077c$. To estimate the initial γ-factor γ_i, we follow electron trajectories in Fig. 3 and record the γ-factor when electrons approach the central axis and enter the laser field moving with the above phase velocity. Our

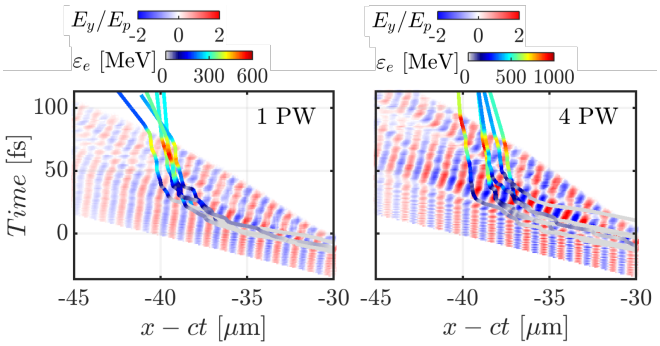

FIG. 3: Temporal profiles of the laser electric field on the central axis ($y = z = 0$). The laser fields are plotted in a moving window together with electron longitudinal trajectories. The left panel is for 1 PW and the right panel is for 4 PW. Note that E_p is the peak electric field corresponding to the laser peak intensity.

estimates of γ_i for 1 and 4 PW are 40 and 100, respectively. Considering the ε_{max} observed in Fig. 1, Eq. (17) gives the transverse boundary as $r_{\rm MB} = 0.93$ μm for 1 PW and $r_{\rm MB} = 1.31$ μm for 4 PW. The estimated boundaries have a good match with the actual amplitude of the transverse oscillations observed in Fig. 2.

In order to determine the role of the superluminosity, we set $u = 1$ in Eq. (17). This effectively removes the last term on the right-hand side that is responsible for the boundary increase with γ. As a result, we obtain significantly smaller values for $r_{\rm MB}$, with $r_{\rm MB} = 0.56$ μm for 1 PW and $r_{\rm MB} = 0.8$ μm for 4 PW. Both values are noticeably smaller than what we observe in the simulations. This comparison unequivocally shows the importance of the superluminosity in electron confinement.

In summary, we have shown that a laser-driven electron can gain energy without increasing the amplitude of its transverse oscillations only while the condition given by Eq. (18) is satisfied. The condition essentially provides a threshold energy corresponding to $\gamma \approx \gamma_i c/(v_{ph}-c)$, where γ_i is the initial electron energy. The amplitude of the transverse oscillations that we call the magnetic boundary radius starts to increase with the electron energy once the value of γ exceeds the threshold value. The non-trivial conclusion is that the threshold is strongly dependent on the superluminosity of the laser.

An important takeaway message from our analytical analysis is that the transverse electron confinement deteriorates with the energy increase, i.e. the boundary expands, and that this deterioration/expansion is a threshold process. In practical terms, this means that there is a significant benefit from a power increase at a constant intensity: the electrons can gain higher energy in a wider beam before being lost due to the boundary expansion. In terms of a single laser system with a given total energy, our results provide an additional consideration when deciding how to focus the laser pulse. The benefits of increasing the peak intensity must be evaluated against the possibility that tighter focusing would lead to premature electron losses during the acceleration process due to a reduced beam width.

This research was supported by AFOSR (Grant No. FA9550-17-1-0382). Simulations were performed with EPOCH (developed under UK EPSRC Grants No. EP/G054940/1, No. EP/G055165/1, and No. EP/G056803/1) using HPC resources provided by TACC at the University of Texas. This work used XSEDE, supported by NSF grant number ACI-1548562.

REFERENCES

[1] H. Daido, M. Nishiuchi, and A. S. Pirozhkov, Reports on Progress in Physics **75**, 056401 (2012).
[2] A. Macchi, M. Borghesi, and M. Passoni, Rev. Mod. Phys. **85**, 751 (2013).
[3] D. Higginson, J. McNaney, D. Swift, G. Petrov, J. Davis, J. Frenje, L. Jarrott, R. Kodama, K. Lancaster, A. Mackinnon, *et al.*, Physics of Plasmas **18**, 100703 (2011).
[4] I. Pomerantz, E. McCary, A. R. Meadows, A. Arefiev, A. C. Bernstein, C. Chester, J. Cortez, M. E. Donovan, G. Dyer, E. W. Gaul, D. Hamilton, D. Kuk, A. C. Lestrade, C. Wang, T. Ditmire, and B. M. Hegelich, Phys. Rev. Lett. **113**, 184801 (2014).
[5] T. Cowan, M. Perry, M. Key, T. Ditmire, S. Hatchett, E. Henry, J. Moody, M. Moran, D. Pennington, T. Phillips, *et al.*, Laser and Particle Beams **17**, 773 (1999).
[6] H. Chen, S. C. Wilks, J. D. Bonlie, E. P. Liang, J. Myatt, D. F. Price, D. D. Meyerhofer, and P. Beiersdorfer, Phys. Rev. Lett. **102**, 105001 (2009).
[7] H. Chen, S. C. Wilks, D. D. Meyerhofer, J. Bonlie, C. D. Chen, S. N. Chen, C. Courtois, L. Elberson, G. Gregori, W. Kruer, O. Landoas, J. Mithen, J. Myatt, C. D. Murphy, P. Nilson, D. Price, M. Schneider, R. Shepherd, C. Stoeckl, M. Tabak, R. Tommasini, and P. Beiersdorfer, Phys. Rev. Lett. **105**, 015003 (2010).
[8] H. Schwoerer, P. Gibbon, S. Düsterer, R. Behrens, C. Ziener, C. Reich, and R. Sauerbrey, Phys. Rev. Lett. **86**, 2317 (2001).
[9] T. Huang, A. Robinson, C. Zhou, B. Qiao, B. Liu, S. Ruan, X. He, and P. Norreys, Physical Review E **93**, 063203 (2016).
[10] D. Stark, T. Toncian, and A. Arefiev, Physical Review Letters **116**, 185003 (2016).
[11] A. Arefiev, V. Khudik, A. Robinson, G. Shvets, L. Willingale, and M. Schollmeier, Physics of Plasmas **23**, 056704 (2016).
[12] A. Pukhov, Z. Sheng, and J. Meyer-ter Vehn, Physics of Plasmas **6**, 2847 (1999).
[13] V. Khudik, A. Arefiev, X. Zhang, and G. Shvets, Physics of Plasmas **23**, 103108 (2016), https://doi.org/10.1063/1.4964901.
[14] A. Arefiev, B. Breizman, M. Schollmeier, and V. Khudik, Phys. Rev. Lett. **108**, 145004 (2012).
[15] A. Arefiev, A. Robinson, and V. Khudik, Journal of Plasma Physics **81**, 475810404 (2015).
[16] O. Jansen, T. Wang, D. J. Stark, E. d'Humières, T. Toncian, and A. V. Arefiev, Plasma Physics and Controlled Fusion **60**, 054006 (2018).